Band gap engineering in MASnBr3 and CsSnBr3 perovskites: mechanistic insights through the application of pressure

Mauro Coduri,[a] Timothy A. Strobel,[b] Marek Szafrański,[c] Andrzej Katrusiak,[d] Arup Mahata,[e,f] Federico Cova,[g] Sara Bonomia, Edoardo Mosconi,[e] Filippo De Angelis,[e,h] and Lorenzo Malavasia,[*]*

a Department of Chemistry and INSTM, Viale Taramelli 16, 27100, Pavia, Italy

b Geophysical Laboratory, Carnegie Institution for Science, Washington, DC 20015, US

c Adam Mickiewicz University, Faculty of Physics, Uniwersytetu Poznańskiego 2, 61-614 Poznań, Poland

d Adam Mickiewicz University, Faculty of Chemistry, Uniwersytetu Poznańskiego 8, 61-614 Poznań, Poland

e Computational Laboratory for Hybrid/Organic Photovoltaics (CLHYO), Istituto CNR di Scienze e Tecnologie Chimiche "Giulio Natta" (CNR-SCITEC), Via Elce di Sotto 8, 06123 Perugia, Italy

f CompuNet, Istituto Italiano di Tecnologia, Via Morego 30, 16163 Genova, Italy

g ESRF – The European Synchrotron, 81, Avenue des Martyrs, 38000, Grenoble, France.

h Department of Chemistry, Biology and Biotechnology, University of Perugia, Via Elce di Sotto 8, 06123 Perugia, Italy

Abstract

Here we report on the first structural and optical high-pressure investigation of $MASnBr_3$ ($MA = [CH_3NH_3]^+$) and $CsSnBr_3$ halide perovskites. A massive red shift of 0.4 eV for $MASnBr_3$ and 0.2 eV for $CsSnBr_3$ is observed within 1.3 to 1.5 GPa from absorption spectroscopy, followed by a huge blue shift of 0.3 and 0.5 eV, respectively. Synchrotron powder diffraction allowed us to correlate the upturn in the optical properties trend (onset of blue shift) with structural phase transitions from cubic to orthorhombic in $MASnBr_3$ and from tetragonal to monoclinic for $CsSnBr_3$. Density functional theory calculations indicate a different underlying mechanism affecting the band gap evolution with pressure, a key role of metal-halide bond lengths for $CsSnBr_3$ and cation orientation for $MASnBr_3$, thus showing the impact of a different A-cation on the pressure response. Finally, the investigated phases, differently from the analogous Pb-based counterparts, are robust against amorphization showing defined diffraction up to the maximum pressure used in the experiments.

The application of an external pressure is a fascinating and powerful tool to manipulate the crystal and electronic structure of any material and has shown great potential for the engineering of photovoltaic (PV) perovskites. (1–5) The interest in high-pressure (HP) research on PV materials is manifold: (i) understand the basic phenomena occurring during hydrostatic/nonhydrostatic compression; (ii) discover new behavior induced by HP; (iii) stabilize new metastable phases; and (iv) try to reproduce the in situ pressure effects by chemical-pressure or the strain induced by a substrate on thin films. (1–5) Starting from the first HP studies on ABX_3 3D hybrid perovskites, other systems have been investigated, namely, double perovskites, 0D perovskite quantum dots or nanocrystals, and layered 2D perovskites. (3)

The most relevant interest in these HP studies, together with the definition of the structural evolution with pressure, is the modulation, or engineering, of the optical band gap (E_g). With reference to 3D perovskites, where the most investigated systems have been $MAPbX_3$ compounds together with $FAPbI_3$, $FAPbBr_3$, and

$CsPbBr_3$, some common HP features of E_g have been observed. (6−17) In particular, the band gap is first red-shifted with *P*, followed by a blue shift, which is usually connected to a structural phase transition to a more distorted crystal structure, if found, within few gigapascals. (2) The proposed mechanism for this trend is well-accepted and considers the first red shift deriving from a shortening of the Pb–X bond length, resulting in increased orbital coupling, whereas the following blue shift arises from local strains generated in the distorted crystal structure, connected to the bending of the Pb–X–Pb bond angles, thus reducing the orbital coupling. (5) This scenario has been developed based on the significant number of papers published on pressure-induced effects on Pb-based perovskites for photovoltaics. However, because of the key role of the perovskite B-atom through its orbital contribution, it is clear that an extension to other systems with different metals should be provided to further understand the level of material properties tunability by substituting the metal atom at the B-site. Moreover, the basic idea of HP studies is to highlight the effect of structural modifications on the band gap, with the aim of engineering them in chemical systems at ambient conditions, apart from investigating the crucially important effects of strains. The search for such effects on lead-free environmentally friendly systems is urgent.

As is well known in the field of PV perovskites, Sn is a natural alternative to Pb. Recently there has been increasing interest toward Sn-based fully inorganic and hybrid perovskites, and an improvement in the PV performance and stability has been achieved. (18,19) Concerning HP studies, only a few Sn-based 3D hybrid perovskite systems have been investigated so far, none of them including Br. (20−22)

In view of the above-reported considerations, in this Letter, we present the results of an HP structural and optical properties investigation on $CsSnBr_3$ and $MASnBr_3$ perovskites carried out in a diamond anvil cell (DAC). The choice of these two systems results from the fact that, recently, $CsSnBr_3$ showed an impressive tolerance toward aging and moisture stability. (23) This suggests that any pressure-induced phenomena could be ideally extended to highly stable Sn(II)-based systems. Moreover, the study of $MASnBr_3$, and the comparison of the behavior between these two systems, sharing the same metal and halogen as well as the same crystal structure at ambient pressure ($Pm\bar{3}m$ space group), could shed some light on the role of the A-site cation (organic or inorganic) on the HP behavior of 3D perovskites, which, based on the available data on Pb-based systems, seems to be dominated by the B-site atom–halogen interaction alone. Finally, the comparison with the Pb-based analogue perovskites, namely, $CsPbBr_3$ and $MAPbBr_3$, will shed light on the role of the B-site metal on the pressure-induced effects. (1,16)

The crystal structure up to 9 GPa was investigated by in situ powder X-ray diffraction (XRD) in a DAC cell with helium as a pressure-transmitting medium. Figure 1 reports some selected integrated XRD patterns for $CsSnBr_3$ and $MASnBr_3$. Details of the measurement strategy together with lattice parameters are reported in the Supporting Information (SI).

Figure 1

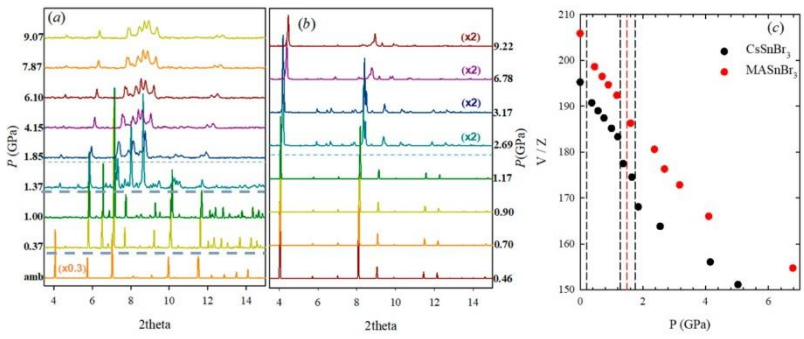

Figure 1. Selected integrated XRD patterns (λ = 0.41116 Å) as a function of pressure (reported in gigapascals on the side) upon compression for (a) $CsSnBr_3$ and (b) $MASnBr_3$. (c) Formula-unit volume as a function of pressure for $CsSnBr_3$ (black) and $MASnBr_3$ (red). Dashed lines highlight phase transitions.

Under ambient conditions $CsSnBr_3$ is cubic (space group $Pm\bar{3}m$) and is reported to exhibit three successive low-temperature phase transformations at 292, 274, and 247 K. (24) We observed that $CsSnBr_3$ already transforms at 0.37 GPa into the tetragonal phase with a primitive unit cell and lattice parameters $a = b = 2$—√ac2ac and $c = 2a_c$, where a_c refers to the cubic unit cell. Consistent with previous low-temperature investigations, the pressure-induced phase has space group $P4/mbm$ and involves the in-phase rotation of the $SnBr_6$ octahedra about the c axis, corresponding to an $a^0a^0c^+$ tilt. (24,25) This phase is isostructural to the high-temperature phase II of $CsPbBr_3$. (26) Another phase transformation occurs above 1.2 GPa, leading to a monoclinic phase with metric $3a_c \cdot 2a_c \cdot 4a_c$. At ∼1.8 GPa, the crystal undergoes a further transition to a more disordered phase, evidenced by a sudden broadening of reflections. (Refined integrated patterns for all of the different crystal structures are reported in Figures S2 and S3.) As shown in Figure 1c, a continuous lattice contraction is observed at HP, with no clear evidence of amorphization. The primitive cubic phase is fully restored after decompression (Figure S4).

The other system investigated (Figure 1b), $MASnBr_3$, shows a single transition at ∼1.5 GPa from the cubic ambient-pressure phase ($Pm\bar{3}m$ space group) to an orthorhombic phase (22—√ac·22—√ac·2ac22ac·22ac·2ac), which is observed up to 9.0 GPa. Again, the cubic phase is restored upon decompression.

Compared with the analogous lead-based perovskites, the structural HP behavior of $CsSnBr_3$ and $MASnBr_3$ is different. Before the pressure-induced amorphization, the $MAPbBr_3$ ambient pressure phase of cubic space group $Pm\bar{3}m$ transforms at 0.75 GPa to another cubic phase of space group $Im\bar{3}$ ($2a \cdot 2a \cdot 2a$), and above 2 GPa to another lower-symmetry phase, probably the orthorhombic space group *Pnma* ($a \cdot 2$—√$a \cdot a$a·2a·a). The cubic and orthorhombic phases coexist in the pressure range 2.1 to 2.7 GPa. (1) A similar evolution upon pressure is observed for other halide perovskites, where the orthorhombic phase is realized either with a doubling of the cubic lattice parameter, leading to the space group *Immm* for $MASnI_3$, or with two parameters along the cubic base diagonals and space group *Pnma*, as observed for $FAPbBr_3$. (17) The $CsPbBr_3$ crystal is of orthorhombic space group *Pnma* at ambient pressure and shows no change of space group until the onset of amorphization at ∼2 GPa, but an isostructural transition was postulated around 1 GPa to reconcile the pressure-induced changes in the absorption edge. (16)

The sequence of HP phases does not match those at low temperature. As a matter of fact, by lowering T, $MASnBr_3$ transforms to a simpler orthorhombic phase (2—√$ac \cdot 2$—√$ac \cdot ac$2ac·2ac·ac), which cannot account for all reflections observed here (Figure S3). (27) Swainson et al. also found a further transformation to a triclinic phase, not observed here. As for $CsSnBr_3$, after the transformation to tetragonal *P4/mbm*, the lower temperature form is orthorhombic *Pnma* rather than monoclinic, as observed here. (24) Hence, some of the HP phases of $CsSnBr_3$ and $MASnBr_3$ do not correspond to the structure reported so far for hybrid perovskites.

Another peculiarity of $CsSnBr_3$ and $MASnBr_3$ is their resistance against amorphization. $MASnBr_3$ is fully crystalline up to 9.2 GPa. The XRD patterns of $CsSnBr_3$ above 2 GPa become broad. However, sharp spots are still observed up to 9.1 GPa, with no evidence of an amorphous-like background. This suggests a sort of microstrain effect, with a wide distribution of lattice parameters rather than amorphization. Another possible explanation is the occurrence of different competing phases, as observed on coesite, which led to

a similar HP broadening. (28) On the contrary, the equivalent Pb-based compounds of the present work, that is, $CsPbBr_3$ and $MAPbBr_3$, show a clear evidence of amorphization starting from ∼2 GPa. (1,16) The occurrence of amorphization is nowadays considered as a driving force for the blue-shifted band gap observed with pressure.

The optical properties under pressure have been measured by photoluminescence (PL) and optical absorbance spectroscopy. The HP PL spectra and the band gap extracted from absorption spectroscopy up to 3 GPa for $CsSnBr_3$ are reported in Figure 2a,b, respectively. Selected optical absorption spectra, together with the positions of PL peaks, are reported in Figures S5–S8. The PL of $CsSnBr_3$ shows a strong signal at ambient pressure at ∼670 nm, in agreement with the available data. (23) This signal red-shifts and increases in intensity with slight application of pressure (0.14 GPa), then diminishes rapidly with no noticeable signal above ∼1.4 GPa (see the inset, logarithmic scale). Notably, this is the pressure around which we found the tetragonal-to-monoclinic phase transition. The red shift evidenced by PL is confirmed by absorption spectroscopy (Figure 2b), where a progressive reduction of the band gap energy is found up to the tetragonal-to-monoclinic phase transition, here observed at ∼1.45 GPa. This behavior has also been observed in $CsPbBr_3$ up to the orthorhombic-to-orthorhombic transition occurring at ∼1.2 GPa. (16) One remarkable difference between the two systems, however, is the magnitude of the red shift. As observed in Figure 2b, the overall variation of E_g from ambient pressure to the phase transition is close to 0.2 eV. In the analogous Pb-based material, the variation is on the order of 0.03 eV; (16) similar red shifts were observed only in 2D perovskites, not before the application of 4 to 5 GPa. (29,30) Following the first red shift, $CsSnBr_3$ has a sudden and impressive blue shift of ∼0.5 eV (Figure 2b). Such a jump in the optical behavior of any fully inorganic or hybrid halide 3D perovskite has never been observed. Usually, there is a smooth upturn from a red shift to a blue shift occurring at a structural change, which is a very general trend irrespective of the crystallographic nature of the two phases involved, (1−5) even though nanostructuring might increase the magnitude of the blue shift. (31,32) When entering the monoclinic phase above ∼1.5 GPa, the band gap has a slight further blue shift up to the existence of a well-defined crystal structure (∼3 GPa, see the XRD data). Above this pressure, the material does not become amorphous, but a significant broadening of the diffraction peaks is found. In this HP regime, the band gap red-shifts progressively up to the highest pressure we could measure (∼10 GPa). Such a trend, even though to lesser extent, has been observed in $MAPbI_3$, where a continuous reduction of the band gap up to (eventually) a metallic state has been observed by conductivity measurements up to 60 GPa. (33) The overall trend of the band gap up to 10 GPa and the corresponding absorption spectra are reported in the SI.

Figure 2

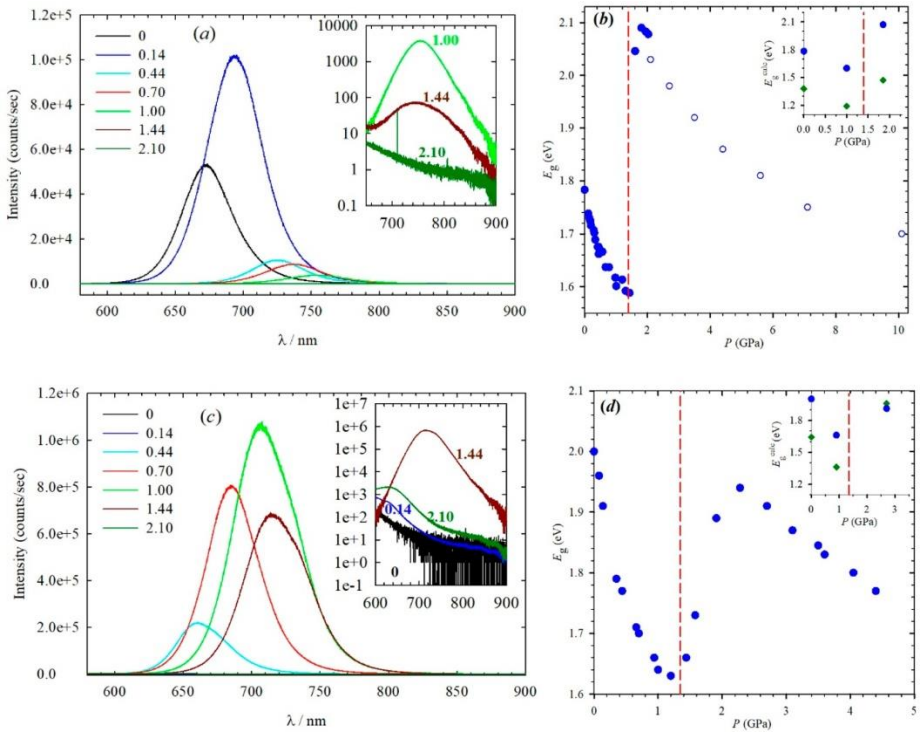

Figure 2. (a) PL spectra and (b) trend of optical band gap versus pressure for $CsSnBr_3$. The vertical dashed line marks the tetragonal-to-monoclinic transition as a medium-pressure Dafne oil was used up to ∼2 GPa (blue circles) and argon was used at higher pressures (empty circles). (c) PL spectra and (d) trend of the optical band gap versus pressure for $MASnBr_3$. The vertical dashed line in panel d marks the region of the cubic-to-orthorhombic phase transition. The insets report in green the band gap values determined ab initio compared with experimental values in blue.

The HP behavior of the optical properties of $MASnBr_3$ are reported in Figure 2c,d. At ambient pressure, the sample shows a weak PL signal with a broad peak near 580 nm, together with a Raman contribution. With increasing pressure, the PL signal red-shifts and increases drastically in intensity up to 1.4 GPa. At ∼ 2 GPa, the PL signal blue-shifts and diminishes in intensity with increasing pressure. The trend of the band gap versus *P* (Figure 2d) confirms the one of PL and extends it up to higher pressures. The upturn in the band gap above ∼1.5 GPa is concomitant to the cubic-to-orthorhombic structural phase transition observed with XRD. Again, the variation of the band gap in the region before the phase transition is huge compared with the Pb-based analogue. For $MASnBr_3$, the change is from ∼2.0 (ambient pressure) to ∼1.6 eV (last before the phase transition), that is, of ∼0.4 eV. On the contrary, the $MAPbBr_3$ system, which is also primitive cubic at ambient pressure, shows an overall red shift of ∼0.04 eV within the ambient phase, whereas it shows a progressive blue shift of ∼0.15 eV from 1 to 3 GPa after the cubic-to-cubic phase transition. (1) We highlight that $MAPbBr_3$ shows strong amorphization already at ∼3 GPa, whereas $MASnBr_3$, after the blue-shift jump (of ∼0.3 eV) at the structural phase transition, shows a continuous red shift of the band gap while retaining the orthorhombic crystal structure without detectable amorphization.

To summarize, $MASnBr_3$ and $CsSnBr_3$ share a common trend of optical properties as a function of pressure: (i) a huge red shift of the band gap in the region before a phase transition, on the order of 0.2 to 0.4 eV, (ii) an abrupt blue-shift jump at the phase transition on the order of 0.3 to 0.5 eV, (iii) a further red shift at higher pressures, and (iv) no appreciable amorphization up to 9 GPa. A comparison of the band gap trend

versus pressure of the Pb-based analogues and the present samples is provided in Figure S9 to highlight the impressive modulation of the band gap of the Sn perovskites compared with the Pb perovskites.

Such an anomalous band gap evolution with pressure was investigated by density functional theory (DFT) calculations, comparing Sn-based perovskites to the analogous perovskites containing Pb. For each system, we optimized the structure at ambient pressure and at the pressures with the lowest and the highest band gaps. The band gap evolution matches nicely with the experimental trends (see the insets in Figure 2b,d), showing a lowering of the band gap with increasing pressure as long as the ambient pressure phase is maintained, followed by a sudden increase in the band gap with pressure, associated with a structure change. The lower absolute band gap in DFT compared with the experiment is due to the sizable structural flexibility of this kind of material. The instantaneous structure could significantly differ from the time scale and experimental XRD structures (i.e., thermal averaged structure). In fact, the dynamic disorder of the A-cation is not decoupled from the inorganic lattice and has important consequences on the electronic properties. (34) Because the motivation of this work is to understand the band gap evolution under pressure, the matching of the absolute values of the band gap with the experiment is not worth considering.

To gain more insight into the shifting of band edges with pressure, we aligned the density of states (DOS, Figure S10) as shown in Figure 3. The valence band maxima (VBM) of ABX_3-type halide perovskites derive from the antibonding hybrid state of the metal s and halide p orbitals, whereas the conduction band minimum (CBM) is a hybrid of metal p and halide p orbitals with less antibonding and more nonbonding character. (35,36) With increasing pressure, the metal-halide bond length decreases (Figure 4a,b), and the overlap between the metal and the halide increases, concomitantly destabilizing the VB. The CB, on the contrary, derives from metal p and halide p orbitals and, having less orbital overlap, responds to a lesser extent than the VB. Both the Pb and Sn perovskites follow this trend irrespective of the A-cation. (See the first two columns of Figure 3.)

Figure 3

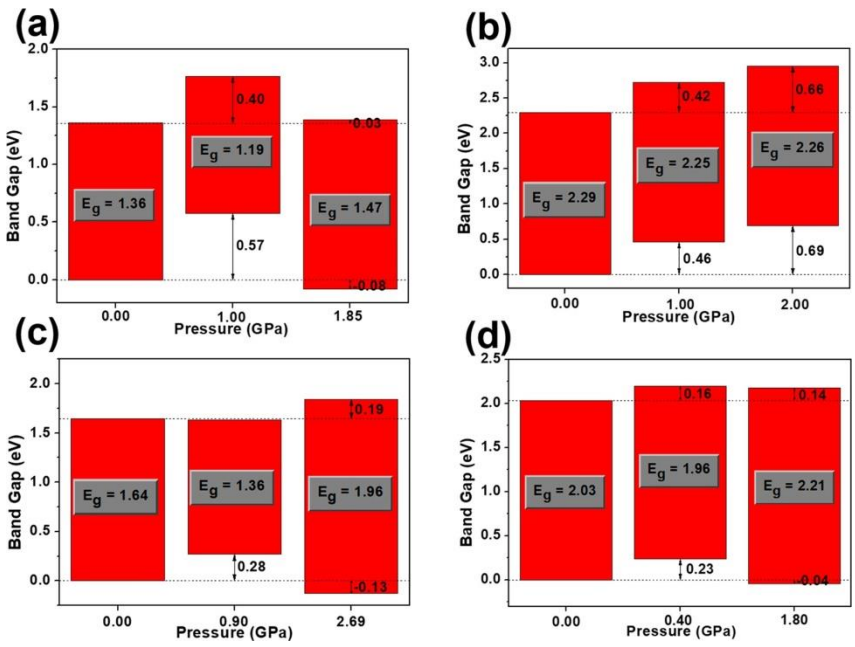

Figure 3. Alignment of band edges under different pressure for (a) $CsSnBr_3$, (b) $CsPbBr_3$, (c) $MASnBr_3$, and (d) $MAPbBr_3$.

Figure 4

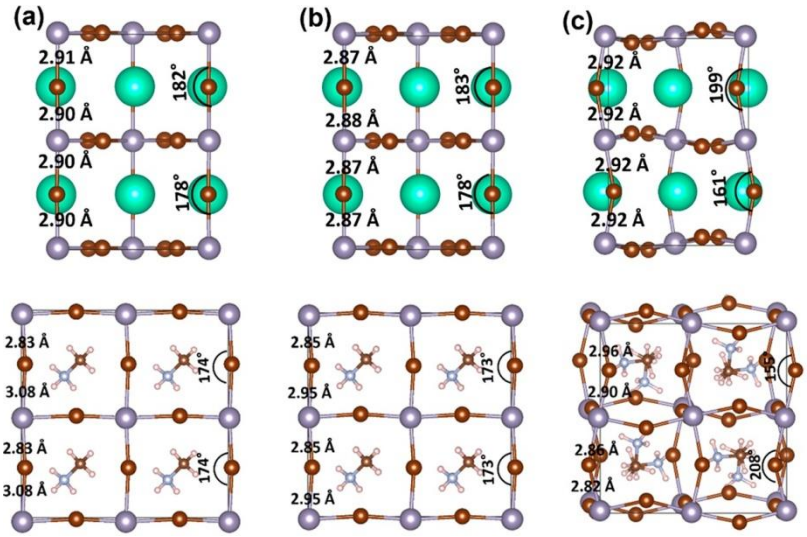

Figure 4. Optimized structures from DFT of $CsSnBr_3$ (top) and $MASnBr_3$ (bottom) at (a) ambient, (b) 1.00 (top) and 0.90 (bottom) GPa, and (c) 1.85 (top) and 2.69 (bottom) GPa.

A further increase in pressure induces the tilting of the metal-halide bond (Figure 4c) concomitant with the phase transformations. The tilting has more impact on the HP behavior of Sn than Pb perovskites. Indeed, in the HP region, the VB of Sn perovskites becomes more stabilized compared with Pb perovskites. As shown in the right panels of Figure 3, the VB is stabilized by 0.65 (from 0.57 to −0.08 eV) and 0.41 eV (from 0.28 to −0.13 eV) for $CsSnBr_3$ and $MASnBr_3$, respectively. On the contrary, only 0.27 eV stabilization is obtained for $MAPbBr_3$, whereas $CsPbBr_3$ is even destabilized. This calls for a careful inspection of the structural and electronic behavior of Pb and Sn perovskites to understand the origin of this contrasting effect.

Let us first consider $CsSnBr_3$. The axial Sn–Br bond length is 2.90 Å at ambient pressure; it shortens to 2.87 Å at 1.00 GPa, and, surprisingly, increases to 2.92 Å by further increasing pressure to 1.85 GPa. Therefore, while moving from cubic to tilted geometry, the Sn–Br bond length increases, thus reducing the Sn–Br overlap and promoting the shifting (by 0.65 eV) of the VB toward lower energies. Notably, the CB also becomes stabilized, but to a lesser extent (0.37 eV). In fact, the stabilization is driven by spin orbit coupling (SOC) only because the nonbonding metal p orbitals character is less influenced by distortion.

The picture gets clearer by considering the Sn content around the CB, which decreases up to 1.00 GPa, followed by an increase up to 1.85 GPa. (See Figure S11 and Table S3.) Because SOC is mainly associated with the heavy Sn centers, it is enhanced by an increase in Sn character. The variable amount of Sn character in the DOS with the tilt angle can be associated with the overlap extent in Sn–Br bonds, which decreases upon octahedral tilting, thus inducing an effective increase in the Sn content up to 5% at the CBM in $CsSnBr_3$. The behavior is marginal at the VB because the SOC contribution of Sn is limited (See Table S3.) However, to further quantify the role of tilting toward the band gap, we considered the case of nontilted geometry maintained at HP. This led to an axial Sn–Br bond distance of 2.88 Å (see Figure S12) with a band gap of 1.12 eV. Therefore, the observed blue shift cannot be obtained without producing a tilted phase with a longer Sn–Br bond distance, which revealed the unusual band gap evolution at HP.

As for the analogous Pb compound, $CsPbBr_3$, the structure remains orthorhombic from ambient pressure throughout the pressure range, (37) showing a contraction of the Pb–Br bond length upon pressure

(see Figure S13), which gradually shifts the VB to higher energies. Similarly, the linear decrease in Pb content (see Text S1) at the CBM destabilizes the CM, thus neutralizing the shift of band edges from the two ends.

As observed for $CsSnBr_3$, also $MASnBr_3$ exhibits band gap reduction under moderate pressure, from 1.64 eV at ambient to 1.36 eV at 0.90 GPa. The band gap becomes higher (1.96 eV) at 2.69 GPa after the cubic-to-orthorhombic phase transition. Notably, the Sn–Br bond distance of pristine $MASnBr_3$ shows an alternating short/long nature of 2.83 to 3.08 Å. However, bond distances possess a typical dynamical average with a shorter time step, as shown for $FASnBr_3$. (38) The short/long nature tends to gradually equalize already at 0.90 GPa (2.85 and 2.95 Å) and at 2.69 GPa (2.86 and 2.91 Å). Therefore, the destabilization of the VB under 0.90 GPa is understandable from the increase in the overlap between Sn–Br bonds, similarly to $CsSnBr_3$. However, at 2.69 GPa the CB shifts to higher energy, a behavior not observed for $CsSnBr_3$. This means that the tilting or the bond length play a limited role in the Sn contribution at the CB. On the contrary, the cation orientation, which is significantly different in the pseudocubic lattice, plays the dominant role toward upshifting the CB by virtue of hydrogen bonding (39) and the Rashba/Dresselhaus effect, (40) which mainly influence the CB. (41) Eventually, $MAPbBr_3$ follows a similar trend as $MASnBr_3$ but smaller in magnitude. This is due to the small difference in the short–long nature of the Pb–Br bond (2.95 and 3.04 Å; see Figure S14) compared with Sn–Br (2.83 and 3.08 Å) together with the prominent SOC effect of Pb compared with Sn. Hence, although the band gap evolution with pressure for both $CsSnBr_3$ and $MASnBr_3$ perovskites is similar, the underlying structural mechanisms are different. The band gap evolution depends on three competing parameters of structural alternations: bond length shortening, octahedral tilting, and cation displacement. All three of these structural alternations occur in parallel; however, one dominates over another depending on the system. In a relatively low-pressure domain, the main parameter is bond-length shortening, whereas at higher pressure octahedral tilting and cation displacement start to play an important role, with the organic cation playing predominant role in hybrid perovskites compared with inorganic perovskites.

To summarize, we reported on the first structural and optical HP investigation of $MASnBr_3$ and $CsSnBr_3$ halide perovskites up to ∼10 GPa by using a DAC under hydrostatic conditions. Massive red shifts of 0.4 eV for $MASnBr_3$ and 0.2 eV for $CsSnBr_3$ are observed from absorption spectroscopy within 1.3 to 1.5 GPa, followed by important blue shifts of 0.3 and 0.5 eV. A further increase in pressure leads to a progressive red shift. Whereas qualitatively, this pressure trend is common to other (mostly Pb-based) hybrid perovskites, the magnitude of red and blue shifts is unprecedented among 3D perovskites for PV applications. The red shift is also confirmed by PL spectra with the PL signal of $MASnBr_3$, which is enhanced at moderate pressure but vanishes at ∼1.5 GPa, concomitantly with the blue shift. Similarly, the PL signal of $CsSnBr_3$ dies out in the same pressure range. The structure evolution with pressure was investigated by synchrotron HP single-crystal diffraction. Both $CsSnBr_3$ and $MASnBr_3$ are cubic under ambient conditions. The upturn in optical properties (the onset of blue shift and PL decay) is consistent with structural changes, namely, from cubic to orthorhombic (∼1.5 GPa) in $MASnBr_3$ and from tetragonal to monoclinic (∼1.3 GPa) in $CsSnBr_3$. The $CsSnBr_3$ crystal exhibits two further transformations: cubic to tetragonal below 0.4 GPa and an isostructural transformation at ∼1.8 GPa toward a more disordered state. The rule of reverse pressure and temperature effects does not hold for these compounds, and the HP crystal phases are different than those reported at low temperature. $CsSnBr_3$ and $MASnBr_3$ are resistant to amorphization, which in other hybrid perovskites generally develops from ∼2 GPa. The structures obtained from XRD were employed as a starting point for DFT calculations, aimed at explaining the origin of the peculiar band gap evolution with pressure. DFT calculations allowed us to describe the band gap evolution as a competition of local structure deformations, such as bond-length shortening, octahedral tilting and cation displacement. Although both

$CsSnBr_3$ and $MASnBr_3$ perovskites show similar band gap evolutions with pressure, the underlying mechanisms are different. The $CsSnBr_3$ band gap is controlled by the Sn–Br bond-length, which contracts with pressure, thus enhancing the orbital overlap with a consequent red shift. Surprisingly, the structural distortion accompanying the phase transformation at ∼1.3 GPa promotes the lengthening of the Sn–Br length, thus reducing the overlap, giving rise to massive blue shift. This applies to $MASnBr_3$ only during red shift, that is, within the stability range of the cubic phase. By further increasing the pressure, the orientational disorder of the organic cation together with the consequent H bonding takes over the Sn–Br bond length to control the electronic properties. This promotes the increase in the CB energy across the cubic-to-orthorhombic transformation, resulting in a blue shift.

Our study shows that the application of external pressure is a powerful tool for tuning the electronic properties of halide perovskites, and, in this respect, $CsSnBr_3$ and $MASnBr_3$ prove to be particularly suitable candidates because their response to external pressure is unprecedented. They are also environmentally friendly alternatives to Pb compounds, thus paving the way for the design of new materials exploring pressure-induced band gap tuning.

Supporting Information

The Supporting Information is available free of charge on the ACS Publications website at DOI: 10.1021/acs.jpclett.9b03046.

Author Information

- **Corresponding Authors**
    - **Filippo De Angelis** - *Computational Laboratory for Hybrid/Organic Photovoltaics (CLHYO), Istituto CNR di Scienze e Tecnologie Chimiche "Giulio Natta" (CNR-SCITEC), Via Elce di Sotto 8, 06123 Perugia, Italy*; *Department of Chemistry, Biology and Biotechnology, University of Perugia, Via Elce di Sotto 8, 06123 Perugia, Italy*; http://orcid.org/0000-0003-3833-1975; Email: filippo.d.angelis@gmail.com
    - **Lorenzo Malavasi** - *Department of Chemistry and INSTM, Viale Taramelli 16, 27100 Pavia, Italy*; http://orcid.org/0000-0003-4724-2376; Email: lorenzo.malavasi@unipv.it
- **Authors**
    - **Mauro Coduri** - *Department of Chemistry and INSTM, Viale Taramelli 16, 27100 Pavia, Italy*; http://orcid.org/0000-0002-5387-8947
    - **Timothy A. Strobel** - *Geophysical Laboratory, Carnegie Institution for Science, Washington, DC 20015, United States*; http://orcid.org/0000-0003-0338-4380
    - **Marek Szafrański** - *Adam Mickiewicz University, Faculty of Physics, Uniwersytetu Poznańskiego 2, 61-614 Poznań, Poland*; http://orcid.org/0000-0001-8178-5222
    - **Andrzej Katrusiak** - *Adam Mickiewicz University, Faculty of Chemistry, Uniwersytetu Poznańskiego 8, 61-614 Poznań, Poland*; http://orcid.org/0000-0002-1439-7278
    - **Arup Mahata** - *Computational Laboratory for Hybrid/Organic Photovoltaics (CLHYO), Istituto CNR di Scienze e Tecnologie Chimiche "Giulio Natta" (CNR-SCITEC), Via Elce di Sotto*

8, 06123 Perugia, Italy; *CompuNet, Istituto Italiano di Tecnologia, Via Morego 30, 16163 Genova, Italy*; http://orcid.org/0000-0002-4995-3326

- **Federico Cova** - *ESRF – The European Synchrotron, 81, Avenue des Martyrs, 38000 Grenoble, France*; http://orcid.org/0000-0002-0130-8299
- **Sara Bonomi** - *Department of Chemistry and INSTM, Viale Taramelli 16, 27100 Pavia, Italy*
- **Edoardo Mosconi** - *Computational Laboratory for Hybrid/Organic Photovoltaics (CLHYO), Istituto CNR di Scienze e Tecnologie Chimiche "Giulio Natta" (CNR-SCITEC), Via Elce di Sotto 8, 06123 Perugia, Italy*

- **Notes**

The authors declare no competing financial interest.

Acknowledgments

We acknowledge the ESRF for the provision of beam time and the help of A. Pisanu and F. Monteforte during data collection. We gratefully acknowledge the project PERSEO "PERrovskite-based Solar cells: towards high Efficiency and lOng-term stability" (Bando PRIN 2015-Italian Ministry of University and Scientific Research (MIUR) Decreto Direttoriale 4 novembre 2015 n. 2488, project number 20155LECAJ) for funding. M.S. is grateful for the financial support from the Polish National Science Centre, Grant Opus 16 No. 2018/31/B/ST3/02188. T.A.S. acknowledges support from EFree, an Energy Frontier Research Center supported by the U.S. Department of Energy, Office of Science, under award no. DE-SC0001057. The authors acknowledge support from the Ministero Istruzione dell'Università e della Ricerca (MIUR) and the University of Perugia through the program "Dipartimenti di Eccellenza 2018-2022" (grant AMIS) and from the European 531 Union's Horizon 2020 research and innovation programme 532 under Grant Agreement No 764047 of the Espresso project.

References

This article references 41 other publications.

1. Szafrański, M.; Katrusiak, A. Photovoltaic Hybrid Perovskites under Pressure. J. Phys. Chem. Lett. 2017, 8, 2496– 2506, DOI: 10.1021/acs.jpclett.7b00520 [ACS Full Text ACS Full Text], [CAS], Google Scholar
2. Postorino, P.; Malavasi, L. Pressure-Induced Effects in Organic–Inorganic Hybrid Perovskites. J. Phys. Chem. Lett. 2017, 8, 2613– 2622, DOI: 10.1021/acs.jpclett.7b00347 [ACS Full Text ACS Full Text], [CAS], Google Scholar
3. Liu, G.; Kong, L.; Yang, W.; Mao, Ho-W Pressure Engineering of Photovoltaic Perovskites. Mater. Today 2019, 27, 91– 106, DOI: 10.1016/j.mattod.2019.02.016 [Crossref], [CAS], Google Scholar
4. Jaffe, A.; Lin, Y.; Karunadasa, H. I. Halide Perovskites Under Pressure: Accessing New Properties through Lattice Compression. ACS Energy. Lett. 2017, 2, 1549– 1555, DOI: 10.1021/acsenergylett.7b00284 [ACS Full Text ACS Full Text], [CAS], Google Scholar

5. Lu, X.; Yang, W.; Jia, Q.; Xu, H. Pressure-induced Dramatic Changes in Organic-Inorganic Halide Perovskites. Chem. Sci. 2017, 8, 6764– 6776, DOI: 10.1039/C7SC01845B [Crossref], [PubMed], [CAS], Google Scholar
6. Wang, K.; Liu, R.; Qiao, Y.; Cui, J.; Song, B.; Liu, B.; Zou, B. Pressure-Induced Reversible Phase Transition and Amorphization of CH3NH3PbI3. 2015, arXiv:1509.03717. arXiv.org e-Print archive. https://arxiv.org/abs/1509.03717 (Accessed April 2019).Google Scholar
7. Ou, T.; Yan, J.; Xiao, C.; Shen, W.; Liu, C.; Liu, X.; Han, Y.; Ma, Y.; Gao, C. Visible Light Response, Electrical Transport, and Amorphization in Compressed Organolead Iodine Perovskites. Nanoscale 2016, 8, 11426– 11431, DOI: 10.1039/C5NR07842C [Crossref], [PubMed], [CAS], Google Scholar
8. Jaffe, A.; Lin, Y.; Beavers, C. M.; Voss, J.; Mao, W. L.; Karunadasa, H. I. High-Pressure Single-Crystal Structures of 3D Lead-Halide Hybrid Perovskites and Pressure Effects on their Electronic and Optical Properties. ACS Cent. Sci. 2016, 2, 201– 209, DOI: 10.1021/acscentsci.6b00055 [ACS Full Text ACS Full Text], [CAS], Google Scholar
9. Jiang, S.; Fang, Y.; Li, R.; Xiao, H.; Crowley, J.; Wang, C.; White, T. J.; Goddard, W. A., III; Wang, Z.; Baikie, T.Pressure-Dependent Polymorphism and Band-Gap Tuning of Methylammonium Lead Iodide Perovskite. Angew. Chem., Int. Ed. 2016, 55, 6540– 6544, DOI: 10.1002/anie.201601788 [Crossref], [CAS], Google Scholar
10. Capitani, F.; Marini, C.; Caramazza, S.; Postorino, P.; Garbarino, G.; Hanfland, M.; Pisanu, A.; Quadrelli, P.; Malavasi, L. High-Pressure Behavior of Methylammonium Lead Iodide (MAPbI3) Hybrid Perovskite. J. Appl. Phys. 2016, 119, 185901, DOI: 10.1063/1.4948577 [Crossref], [CAS], Google Scholar
11. Szafranski, M.; Katrusiak, A. Mechanism of Pressure-induced Phase Transitions, Amorphization, and Absorption-Edge Shift in Photovoltaic Methyammonium Lead Iodide. J. Phys. Chem. Lett. 2016, 7, 3458– 3466, DOI: 10.1021/acs.jpclett.6b01648 [ACS Full Text ACS Full Text], [CAS], Google Scholar
12. Swainson, I. P.; Tucker, M. G.; Wilson, D. J.; Winkler, B.; Milman, V. Pressure Response of an Organic-inorganic Perovskite: Methylammonium Lead Bromide. Chem. Mater. 2007, 19, 2401– 2405, DOI: 10.1021/cm0621601 [ACS Full Text ACS Full Text], [CAS], Google Scholar
13. Wang, Y.; Lu, X.; Yang, W.; Wen, T.; Yang, L.; Ren, X.; Wang, L.; Lin, Z.; Zhao, Y. Pressure-Induced Phase Transformation, Reversible Amorphization and Anomalous Visible Light Response in Organolead Bromide Perovskite. J. Am. Chem. Soc. 2015, 137, 11144– 11149, DOI: 10.1021/jacs.5b06346 [ACS Full Text ACS Full Text], [CAS], Google Scholar
14. Wang, L.; Wang, K.; Xiao, G.; Zeng, Q.; Zou, B. Pressure-Induced Structural Evolution and Band Gap Shifts of Organometal Halide Perovskite-Based Methylammonium Lead Chloride. J. Phys. Chem. Lett. 2016, 7, 5273– 5279, DOI: 10.1021/acs.jpclett.6b02420 [ACS Full Text ACS Full Text], [CAS], Google Scholar
15. Wang, P.; Guan, J.; Galeschuk, T. K.; Yao, Y.; He, C. F.; Jiang, S.; Zhang, S.; Liu, Y.; Jin, M.; Jin, C.; Song, Y. Pressure-Induced Polymorphic, Optical, and Electronic Transitions of Formamidinium Lead Iodide Perovskite. J. Phys. Chem. Lett. 2017, 8, 2119– 2125, DOI: 10.1021/acs.jpclett.7b00665 [ACS Full Text ACS Full Text], [CAS], Google Scholar
16. Zhang, L.; Zeng, Q.; Wang, K. Pressure-Induced Structural and Optical Properties of Inorganic Halide Perovskite CsPbBr3. J. Phys. Chem. Lett. 2017, 8, 3752– 3758, DOI: 10.1021/acs.jpclett.7b01577 [ACS Full Text ACS Full Text], [CAS], Google Scholar
17. Wang, L.; Wang, K.; Zou, B. Pressure-Induced Structural and Optical Properties of Organometal Halide Perovskite-Based Formamidinium Lead Bromide. J. Phys. Chem. Lett. 2016, 7, 2556– 2562, DOI: 10.1021/acs.jpclett.6b00999 [ACS Full Text ACS Full Text], [CAS], Google Scholar

18. Song, T.-B.; Yokoyama, T.; Aramaki, S.; Kanatzidis, A. G. Performance Enhancement of Lead-Free Tin-Based Perovskite Solar Cells with Reducing Atmosphere-Assisted Dispersible Additive. ACS Energy Lett. 2017, 2, 897– 903, DOI: 10.1021/acsenergylett.7b00171 [ACS Full Text ACS Full Text], [CAS], Google Scholar
19. Gupta, S.; Bendikov, T.; Hodes, G.; Cahen, D. CsSnBr3, A Lead-Free Halide Perovskite for Long-Term Solar Cell Application: Insights on SnF2 Addition. ACS Energy Lett. 2016, 1, 1028– 1033, DOI: 10.1021/acsenergylett.6b00402 [ACS Full Text ACS Full Text], [CAS], Google Scholar
20. Lu, X.; Wang, Y.; Stoumpos, C. C.; Hu, Q.; Guo, X.; Chen, H.; Yang, L.; Smith, J. S.; Yang, W.; Zhao, Y.; Xu, H.; Kanatzidis, M. G.; Jia, Q. Enhanced Structural Stability and Photo Responsiveness of CH3NH3SnI3 Perovskite via Pressure-Induced Amorphization and Recrystallization. Adv. Mater. 2016, 28, 8663– 8668, DOI: 10.1002/adma.201600771 [Crossref], [PubMed], [CAS], Google Scholar
21. Wang, L.; Ou, T.; Wang, K.; Xiao, G.; Gao, C.; Zou, B. Pressure-Induced Structural Evolution, Optical and Electronic Transitions of Nontoxic Organometal Halide Perovskite-Based Methylammonium Tin Chloride. Appl. Phys. Lett. 2017, 111, 233901, DOI: 10.1063/1.5004186 [Crossref], [CAS], Google Scholar
22. Lee, Y.; Mitzi, D. B.; Barnes, P. W.; Vogt, T. Pressure-induced Phase Transitions and Templating Effect in Three-dimensional Organic-inorganic Hybrid Perovskites. Phys. Rev. B: Condens. Matter Mater. Phys. 2003, 68, 020103(R) DOI: 10.1103/PhysRevB.68.020103 [Crossref], Google Scholar
23. Bernasconi, A.; Rizzo, A.; Listorti, A.; Mahata, A.; Mosconi, E.; De Angelis, F.; Malavasi, L. Synthesis, Properties, and Modeling of Cs1–xRbxSnBr3 Solid Solution: A New Mixed-Cation Lead-Free All-Inorganic Perovskite System. Chem. Chem. Mater. 2019, 31, 3527– 3533, DOI: 10.1021/acs.chemmater.9b00837 [ACS Full Text ACS Full Text], [CAS], Google Scholar
24. Fabini, D. H.; Laurita, G.; Bechtel, J. S.; Stoumpos, C. C.; Evans, H. A.; Kontos, A. G.; Raptis, Y. S.; Falaras, P.; Van der Ven, A.; Kanatzidis, M. G.; Seshadri, R. Dynamic Stereochemical Activity of the Sn2+ Lone Pair in Perovskite CsSnBr3. J. Am. Chem. Soc. 2016, 138, 11820– 11832, DOI: 10.1021/jacs.6b06287 [ACS Full Text ACS Full Text], [CAS], Google Scholar
25. Mori, M.; Saito, H. An x-ray study of successive phase transitions in CsSnBr3. J. Phys. C: Solid State Phys. 1986, 19, 2391– 2401, DOI: 10.1088/0022-3719/19/14/005 [Crossref], [CAS], Google Scholar
26. Hirotsu, S.; Harada, J.; Iizumi, M.; Gesi, K. Structural phase transitions in CsPbBr3. J. Phys. Soc. Jpn. 1974, 37, 1393– 1398, DOI: 10.1143/JPSJ.37.1393 [Crossref], [CAS], Google Scholar
27. Swainson, I.; Chi, L.; Her, J.-H.; Cranswick, L.; Stephens, P.; Winkler, B.; Wilson, D. J.; Milman, V. Orientational Ordering, Tilting and Lone-pair Activity in the Perovskite Methylammonium Tin Bromide, CH3NH3SnBr3. Acta Crystallogr., Sect. B: Struct. Sci. 2010, 66, 422– 429, DOI: 10.1107/S0108768110014734 [Crossref], [PubMed], [CAS], Google Scholar
28. Hu, Q. Y.; Shu, J.-F.; Cadien, A.; Meng, Y.; Yang, W. G.; Sheng, H. W.; Mao, H.-K. Polymorphic Phase Transition Mechanism of Compressed Coesite. Nat. Commun. 2015, 6, 6630, DOI: 10.1038/ncomms7630 [Crossref], [PubMed], [CAS], Google Scholar
29. Liu, G.; Kong, L.; Guo, P.; Stoumpos, C. C.; Hu, Q.; Liu, Z.; Cai, Z.; Gosztola, D. J.; Mao, H.-K.; Kanatzidis, M. G.; Schaller, R. D. Two Regimes of Bandgap Red Shift and Partial Ambient Retention in Pressure-Treated Two-Dimensional Perovskites. ACS Energy Lett. 2017, 2 (11), 2518– 2524, DOI: 10.1021/acsenergylett.7b00807 [ACS Full Text ACS Full Text], [CAS], Google Scholar
30. Yin, T.; Liu, B.; Yan, J.; Fang, Y.; Chen, M.; Chong, W. K.; Jiang, S.; Kuo, J.-L.; Fang, J.; Liang, P.; Wei, S.; Loh, K. P.; Sum, T. C.; White, T. J.; Shen, Z. X. Pressure-Engineered Structural and Optical Properties of Two-Dimensional (C4H9NH3)2PbI4 Perovskite Exfoliated nm-Thin Flakes. J. Am. Chem. Soc. 2019, 141 (3), 1235– 1241, DOI: 10.1021/jacs.8b07765 [ACS Full Text ACS Full Text], [CAS], Google Scholar

31. Xiao, G.; Cao, Y.; Qi, G.; Wang, L.; Liu, C.; Ma, Z.; Yang, X.; Sui, Y.; Zheng, W.; Zou, B. Pressure Effects on Structure and Optical Properties in Cesium Lead Bromide Perovskite Nanocrystals. J. Am. Chem. Soc. 2017, 139 (29), 10087– 10094, DOI: 10.1021/jacs.7b05260 [ACS Full Text ACS Full Text], [CAS], Google Scholar
32. Zhu, H.; Cai, T.; Que, M.; Song, J.-P.; Rubenstein, B. M.; Wang, Z.; Chen, O. Pressure-Induced Phase Transformation and Band-Gap Engineering of Formamidinium Lead Iodide Perovskite Nanocrystals. J. Phys. Chem. Lett. 2018, 9 (15), 4199– 4205, DOI: 10.1021/acs.jpclett.8b01852 [ACS Full Text ACS Full Text], [CAS], Google Scholar
33. Jaffe, A.; Lin, Y.; Mao, W. L.; Karunadasa, H. I. Pressure-Induced Metallization of the Halide Perovskite (CH3NH3)PbI3. J. Am. Chem. Soc. 2017, 139, 4330– 4333, DOI: 10.1021/jacs.7b01162 [ACS Full Text ACS Full Text], [CAS], Google Scholar
34. Quarti, C.; Mosconi, E.; De Angelis, F. Structural and electronic properties of organo-halide hybrid perovskites from ab initio molecular dynamics. Phys. Chem. Chem. Phys. 2015, 17, 9394, DOI: 10.1039/C5CP00599J [Crossref], [PubMed], [CAS], Google Scholar
35. Lee, J. H.; Bristowe, N. C.; Lee, J. H.; Lee, S. H.; Bristowe, P. D.; Cheetham, A. K.; Jang, H. M. Resolving the Physical Origin of Octahedral Tilting in Halide Perovskites. Chem. Mater. 2016, 28, 4259– 4266, DOI: 10.1021/acs.chemmater.6b00968 [ACS Full Text ACS Full Text], [CAS], Google Scholar
36. Grote, C.; Berger, R. F. Strain Tuning of Tin–Halide and Lead–Halide Perovskites: A First-Principles Atomic and Electronic Structure Study,. J. Phys. Chem. C 2015, 119, 22832– 22837, DOI: 10.1021/acs.jpcc.5b07446 [ACS Full Text ACS Full Text], [CAS], Google Scholar
37. Zhang, L.; Zeng, Q.; Wang, K. Pressure-Induced Structural and Optical Properties of Inorganic Halide Perovskite CsPbBr3. J. Phys. Chem. Lett. 2017, 8, 3752– 3758, DOI: 10.1021/acs.jpclett.7b01577 [ACS Full Text ACS Full Text], [CAS], Google Scholar
38. Pisanu, A.; Mahata, A.; Mosconi, E.; Patrini, M.; Quadrelli, P.; Milanese, C.; De Angelis, F.; Malavasi, L. Exploring the Limits of Three-Dimensional Perovskites: The Case of FAPb1–xSnxBr3. ACS Energy Lett. 2018, 3, 1353– 1359, DOI: 10.1021/acsenergylett.8b00615 [ACS Full Text ACS Full Text], [CAS], Google Scholar
39. Amat, A.; Mosconi, E.; Ronca, E.; Quarti, C.; Umari, P.; Nazeeruddin, M. K.; Grätzel, M.; De Angelis, F. Cation-Induced Band-Gap Tuning in Organohalide Perovskites: Interplay of Spin–Orbit Coupling and Octahedra Tilting. Nano Lett. 2014, 14, 3608– 3616, DOI: 10.1021/nl5012992 [ACS Full Text ACS Full Text], [CAS], Google Scholar
40. Quarti, C.; Mosconi, E.; De Angelis, F. Interplay of Orientational Order and Electronic Structure in Methylammonium Lead Iodide: Implications for Solar Cell Operation. Chem. Mater. 2014, 26, 6557– 6569, DOI: 10.1021/cm5032046 [ACS Full Text ACS Full Text], [CAS], Google Scholar
41. Etienne, T.; Mosconi, E.; De Angelis, F. Dynamical Origin of the Rashba Effect in Organohalide Lead Perovskites: A Key to Suppressed Carrier Recombination in Perovskite Solar Cells?. J. Phys. Chem. Lett. 2016, 7, 1638– 1645, DOI: 10.1021/acs.jpclett.6b00564 [ACS Full Text ACS Full Text], [CAS], Google Scholar